Soft Matter

Cite this: *Soft Matter*, 2011, **7**, 5745

www.rsc.org/softmatter

PAPER

Dynamics of water confined to reverse AOT micelles

Tinka Luise Spehr,*[ab] Bernhard Frick,[b] Michaela Zamponi[cd] and Bernd Stühn[a]

Received 8th February 2011, Accepted 30th March 2011
DOI: 10.1039/c1sm05204g

We use quasi-elastic neutron scattering (QENS) to study the dynamics of water confined inside reverse micelles. As a model system we use a water-in-oil droplet microemulsion based on the anionic surfactant AOT (sodium bis[2-ethylhexyl] sulfosuccinate), that forms spherical water droplets coated by a monolayer of AOT dispersed in the continuous oil matrix. Combining neutron time-of-flight (TOF) and backscattering (BS) spectroscopy, we access the dynamical behaviour of water over three decades in time from pico- to nanoseconds. We investigate the influence of reverse micelle size on the water dynamics by comparing two sample systems with bigger and smaller water core radii of about $R_c \approx 12$ Å and 7 Å. The temperature is varied over a range where both microemulsion systems are stable, from room temperature down to the region where the confined water is supercooled: 260 K $\leq T \leq$ 300 K. Taking explicitly into account the previously measured diffusion of entire reverse micelles in the oil matrix we find the average mobility of the confined water to be considerably slowed with respect to bulk water. The translational diffusion decreases with decreasing reverse micelle size. Dependent on the reverse micelle size we can interpret our data by assuming two dynamically separated water fractions. We identify the faster one with bulk-like water in the middle of the core while the slower one seems to be surfactant bound water. We find that 4 molecules of water per AOT molecule are immobilized on the timescale of QENS, *i.e.* shorter than nanoseconds.

1 Introduction and background

The behaviour of liquids and especially water in confinement is the subject of intense research motivated by applications as well as by fundamental questions.[1–4] The dynamics of confined water has been studied in hard confinement for example in porous silica,[5,6] clay materials[7] or carbon nanotubes.[8]

However, within recent years the great importance of wall interactions with the confined liquids became evident.[1–4] Besides the geometry of the confinement also the water–substrate interaction (hydrophilic or hydrophobic) plays a crucial role for the modification of the water behaviour and its spatial range.[9] With these observations the interest developed to modify wall properties either by coating the nanoporous host walls or more recently by studying liquids enclosed within soft walls.[10–12] Such soft walls can be realized in microemulsions. In these mixtures of polar and apolar liquids, mediated by surfactants, one possible structure is that of spherical water droplets coated by a monolayer of surfactant that are dispersed in a continuous oil matrix. Such a water-containing reverse micelle is sketched in Fig. 1: the surfactant molecules are pointing with their hydrophilic head groups towards the micellar water core, their tails are dissolved in the oil, so that the surfactant forms a soft shell that separates both liquids. For the study of the contained water, the reverse micelles offer the advantage that important parameters like the degree of confinement (by the micelle size[13]) and probably also the hardness of the confinement (by rigidity of the surfactant shell[14]) may be varied systematically. Besides the reason to better control confinement and wall interaction, microemulsions are chosen as model systems because of their similarity with systems of biological relevance.

One of the best characterized water-in-oil droplet microemulsions is based on the anionic surfactant AOT (sodium bis [ethylhexyl] sulfosuccinate).[15–17] For a given surfactant concentration the size of the water core increases linearly with increasing water content[13] so that one may prepare droplets with radii

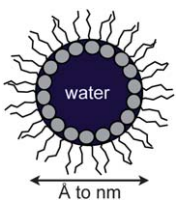

Fig. 1 Water-swollen reverse micelle.

[a]*Institut für Festkörperphysik, Technische Universität Darmstadt, 64289 Darmstadt, Germany. E-mail: tinka.spehr@physik.tu-darmstadt.de; Fax: +49 6151 164883; Tel: +49 6151 162483*
[b]*Institut Laue-Langevin, 6, rue Horowitz, 38042 Grenoble, France*
[c]*Jülich Centre for Neutron Science, Forschungszentrum Jülich, 52425 Jülich, Germany*
[d]*Spallation Neutron Source, Oak Ridge National Laboratory, Oak Ridge, TN, 37831, USA*

between a few Ångströms up to several nanometres for certain oils. For moderate water content the w/o droplet microemulsion is stable down to temperatures below the freezing point of bulk water, allowing the study of the enclosed water in the supercooled state.[18,19]

Well-suited methods to study the dynamical behaviour of confined water are quasi-elastic neutron scattering (QENS) techniques.[20] Provided that the predominant incoherent contribution to the scattering is due to the water in the sample, QENS measures the incoherent dynamic scattering function $S(Q, \omega)$ which is through Fourier transforms related to the self-correlation function of the water protons.[20] The combination of different neutron spectrometers provides access to time scales from picoseconds to nanoseconds with the spatial experimental resolution matching the spacings relevant for the water motion, so that rotational as well as translational diffusion of the water molecules may be investigated. Exploiting the range of accessible scattering vectors $Q = \frac{4\pi}{\lambda}\sin(\theta)$ with the neutron wavelength λ and the scattering angle 2θ, the distinction between different models for the motion becomes possible. Neutron scattering is a non-destructive method and therefore the structure and dynamics of the sample under investigation are unaltered by the scattering process and one may study the water directly without introducing a probe molecule as has to be done *e.g.* with fluorescence probing.[21]

In this paper we report results on the dynamical behaviour of water confined to reverse AOT micelles. We use QENS to study the water's translational and rotational motion combining three different neutron spectrometers. We discuss the measured intermediate scattering function in terms of the jump diffusion model for the translational part and the Sears model for the rotational part. Special attention is paid to distinguish between reverse micelle dynamics and water motion. For this purpose we refer to a recent neutron spin echo study where we have obtained absolute micelle diffusion coefficients for the here used microemulsions.[19] Exploiting the longest accessed times we are able to distinguish between two dynamically separated water fractions. We compare our findings to results for bulk water and water confined by different environments.

1.1 Theoretical basics and fitting model

Water molecules undergo vibrational, translational and rotational motion. For the time and spatial range probed by QENS these different kinds of motions appear as decoupled and hence the measured total incoherent dynamic structure factor $S(Q, \omega)$ is the convolution product of the vibrational, translational and rotational parts.[6,11,22] Experimentally the dynamic scattering function is probed (convoluted) with the instrument specific resolution function $R(Q, \omega)$. In the time domain the intermediate scattering function is then a simple product of the respective parts:

$$I(Q,t) = I_V(Q,t)\cdot I_T(Q,t)\cdot I_R(Q,t)\cdot R(Q,t) \quad (1)$$

In the quasi-elastic region (timescale of picoseconds and longer) the vibrational dynamics have decayed and their apparent contribution to the scattered intensity can very well be approximated by a Debye–Waller factor:[20]

$$I_V(Q,t) = I_V(Q) \approx \exp\left(-\frac{1}{3}Q^2\langle u^2\rangle\right) \quad (2)$$

with $\langle u^2\rangle$ denoting the mean square vibrational amplitude of a hydrogen atom around its equilibrium position. For water in hard confinement a vibrational amplitude of $\sqrt{\langle u^2\rangle} \leq 0.1$ Å was assumed by Liu *et al.* and then the Debye–Waller factor can be set to unity for the range probed by QENS.[6] As an estimation for an upper limit for the vibrational contribution we calculate $I_V(Q, t)$ with $\sqrt{\langle u^2\rangle} = 0.48$ Å as determined by Teixeira and co-workers for free bulk water.[23] At the highest Q of interest in this work ($Q_{max} \approx 1.2$ Å^{-1}, see section 2.2) $I_V(Q, t)$ would then decay to 90% of the value at $Q = 0$. In the following any possible vibrational contributions to the scattering will be included in a scaling factor that also contains intensity variations due to normalization with resolution spectra of crystallized samples and possible coherent contributions. We will desist from drawing any conclusions on the vibrational motion of water from our experiments.

The translational motion of water results in an exponentially decaying intermediate scattering function:

$$I_T(Q,t) = \exp(-\Gamma_T t) \quad (3)$$

In the frequency domain this yields a Lorentzian shaped dynamic structure factor with a half width at half maximum HWHM = Γ_T, where Γ_T would vary as $\Gamma_T(Q) = D_T Q^2$.

The model of isotropic free translational diffusion is often insufficient to describe the measured scattering functions of diffusing particles. When the probed Q is larger than the inverse of the distance between neighboring molecules the neutrons will also detect the microscopic details of the diffusion process. In the case of water, the translational diffusion is in this range successfully described by a random jump diffusion model presented first by Singwi and Sjölander.[24] The molecules alternately undergo oscillatory motion inside a cage of neighbors for a residence time τ_0 and free diffusion for a time τ_1, until they are trapped in a different neighborhood. Assuming that the oscillation time is much longer than the diffusion time, *i.e.* $\tau_1 \ll \tau_0$, Γ_T varies according to:

$$\Gamma_T(Q) = \frac{D_T Q^2}{1 + D_T Q^2 \tau_0} \quad (4)$$

with the translational diffusion coefficient D_T.[20] Since the pioneering work of Teixeira and co-workers on bulk water,[23] this model has successfully been applied to describe the translational part of QENS data for water in many different environments.

For the rotational motion we apply the Sears model for a molecule rotating on a sphere of radius a.[25] The corresponding intermediate scattering function is an infinite sum over exponential functions weighted by the quasi-elastic structure factors $A_l(Qa)$ plus an elastic part $A_0(Qa)$ due to the spatial restriction to the sphere:

$$I_R(Q,t) = A_0(Qa) + \sum_{l=1}^{\infty} A_l(Qa)\cdot\exp\left[-\frac{t}{\tau_l}\right] \quad (5)$$

with the quasi-elastic structure factors $A_l(Qa)$ being defined as follows:

$$A_0(Qa) = [j_0(Qa)]^2 \quad (6)$$

$$A_l(Qa) = (2l + 1)[j_1(Qa)]^2 \quad (7)$$

j_l denotes the spherical Bessel function of order l. For water protons the radius of rotation corresponds to the length of an O–H bond, $a \approx 0.98$ Å. The correlation time τ_l of order l is related to the rotational diffusion coefficient $D_R = [l(l + 1)\tau_l]^{-1}$. When speaking of the rotational time τ_R one generally refers to the second order correlation time $\tau_R = \tau_2 = 1/(6D_R)$.

In practice for the fitting of our measured QENS data the infinite sum in the rotational part can be truncated after a few terms as the intensity of the higher order terms is negligible for the experimentally accessible Q range. We take into account only the first three rotational terms up to $l = 2$. Discussing the measured data in the time domain offers the advantage that we can simply divide out the instrument specific resolution $R(Q, t)$ and the intermediate scattering functions of the three spectrometers may then be combined to yield one $I(Q, t)$. The instrumental resolution spectra are measured on the partly crystalline sample which introduces an intensity variation that is difficult to quantify and that will be considered in a scaling factor K in eqn (8) which also includes the scaling of the total quasi-elastic intensity due to vibrations and coherent contributions. Altogether the total resolution-corrected intermediate scattering function for rotational–translational water motion then reads:

$$\begin{aligned} I(Q,t) &= K \cdot I_T(Q,t) \cdot I_R(Q,t) \\ &= K \cdot A_0(Qa) \cdot \exp[-\Gamma_T t] \\ &+ K \cdot \sum_{l=1}^{2} A_l(Qa) \cdot \exp\left[-\left(\Gamma_T + \tau_l^{-1}\right)t\right] \end{aligned} \quad (8)$$

2 Experimental

2.1 Samples and materials

Water-in-oil droplet microemulsions were prepared by mixing appropriate amounts of AOT, water and d-toluene and shaking for several minutes until the samples were single-phase and optically clear. D_2O (Euriso-top, >99.9%) and toluene-d_8 (Acros Organics, >98%) were used without further purification. Deuterated AOT-d_{34} was purchased from R. Thomas, Oxford. De-ionized water was taken from a Millipore Direct-Q3 system. The composition of the microemulsions is characterized by ω and ϕ, with ω being the molar ratio of water to surfactant AOT and ϕ being the droplet (water plus AOT) volume fraction. The droplet water core radius depends to a first approximation linearly on ω and is for moderate droplet concentrations independent of ϕ.[13] Here we work with two sets of H_2O/d-AOT/toluene-d_8 microemulsions with $\omega = 3$ and $\omega = 8$ and constant volume fraction of $\phi = 0.1$. In a previous study we have used small-angle neutron scattering (SANS) to determine the respective water core radii of these two systems to $R_c = 7$ Å and $R_c = 12$ Å.[19] The droplet structure remains unchanged down to temperatures below $T \approx 235$ K for the smaller reverse micelles and $T \approx 260$ K for the bigger ones.[19] For both droplet sizes fully deuterated background samples with otherwise identical compositions ($\omega = 3$, $\omega = 8$ and $\phi = 0.1$) were measured.

2.2 Instruments and data corrections

We combined three different QENS spectrometers, a listing of the instrumental characteristics is given in Table 1.

2.2.1 TOF spectrometer IN5. The first measurement was done at the TOF spectrometer IN5 at the ILL, Grenoble. With an incident wavelength of $\lambda = 8$ Å the investigated scattering vector is 0.3 Å^{-1} < Q < 1.45 Å^{-1}. The tested energy transfer is −5 meV < ΔE < +0.5 meV with an instrumental resolution (FWHM) of $\delta E = 20 - 25$ μeV. Flat aluminum sample holders with a wall to wall thickness of 1 mm were used and the sample was positioned at 135° with respect to the incident beam. All spectra were collected for at least 2 h, up to 4 h for the background samples. At each of the five investigated temperatures between $T = 260$ K and 300 K we have interpolated constant scattering angle data and obtained a set of $S(Q, \omega)$ with Q increasing in steps of 0.05 Å^{-1} from the minimum $Q = 0.3$ Å^{-1} on. We took into account only spectra up to $Q = 1.1$ Å^{-1}. For higher Q, artifacts due to Fourier transformation of the data become more and more important because of the finite accessed energy. Moreover by restricting the data analysis to this Q range we avoided the interval where the maximum of the structure factor of liquid D_2O is located.

2.2.2 TOF-BS spectrometer BASIS. A second experiment was performed on the TOF-BS instrument BASIS at the SNS, ORNL. Using an incident wavelength of $\lambda = 6.4$ Å (chopper frequency of 60 Hz) the tested scattering vector ranged from 0.2 Å^{-1} < Q < 2 Å^{-1}. The instrumental resolution was $\delta E \approx$ 3.4 μeV and the selected energy transfer ranged from −180 μeV < ΔE < +180 μeV. Hollow cylindrical aluminum sample holders allowing for a sample wall thickness of 0.25 mm were used. For temperatures $T = 270$ K, 280 K and 290 K we obtained a set of $S(Q, \omega)$ with Q increasing in steps of 0.2 Å^{-1} from the minimum $Q = 0.3$ Å^{-1} on. Spectra up to $Q = 1.1$ Å^{-1} will be considered.

Table 1 Summary of performed QENS experiments. λ_i denotes the incident neutron wavelength, δE is the instrumental resolution (FWHM). The given energy transfer ΔE and elastic Q range correspond to evaluable spectra, the instrumental accessible range differs.

Instrument	λ_i/Å	δE/μeV	ΔE/μeV	T/K	Q/Å^{-1}
IN5	8	20–25	−5000 to +500	300, 290, 280, 270, 260	0.3–1.1
BASIS	6.4	3.4	−120 to +120	290, 280, 270	0.3–1.1
IN16	6.271	<1	−15 to +15	270	0.3–0.5

2.2.3 BS spectrometer IN16. The third experiment was performed on the BS spectrometer IN16 at the ILL. With an incident wavelength of $\lambda = 6.271$ Å an elastic Q range of $0.2\ \text{Å}^{-1} < Q < 1.9\ \text{Å}^{-1}$ was probed. The instrumental energy resolution was $\delta E = 0.9$ μeV and the accessible energy transfer ranged from $-15\ \mu\text{eV} < \Delta E < +15\ \mu\text{eV}$. The spectra have been measured at a single temperature of $T = 270$ K with a collecting time of about 12 h per sample. The same sample holders as for IN5 were used, also positioned at 135° with respect to the incident beam.

At all three instruments we use vanadium spectra for normalization and to correct for detector efficiency. Sample spectra at $T \leq 10$ K serve to determine the instrumental resolution $R(Q, \omega)$. The calculated transmissions of all samples are higher than 0.86 and we do not apply multiple scattering corrections. The difference of the corrected measured dynamic scattering functions $S(Q, \omega)$ of sample and background sample are Fourier transformed to yield the intermediate scattering function $I(Q, t)$ using the Fourier transform algorithm *unifit* provided by R. Zorn, Jülich.

3 Results

As the first step towards an overall description of the data from all three instruments we analyze the data of IN5, where we have obtained the largest number of spectra (concerning scattering vector Q and temperature T) with the best statistics. The results will then be used to constrict parameters for the analysis of the data from BASIS and IN16.

The fitting of $I(Q, t)$ measured on IN5 is done in two stages. First, each set of data is fitted to eqn (8) with a fixed $a = 0.98$ Å. For each temperature we perform a global fit of all $I(Q, t)$ obtained from IN5 for different Q: the rotational diffusion coefficient D_R is simultaneously optimized over the entire Q range investigated whereas the translational width Γ_T is for each Q value fitted independently.

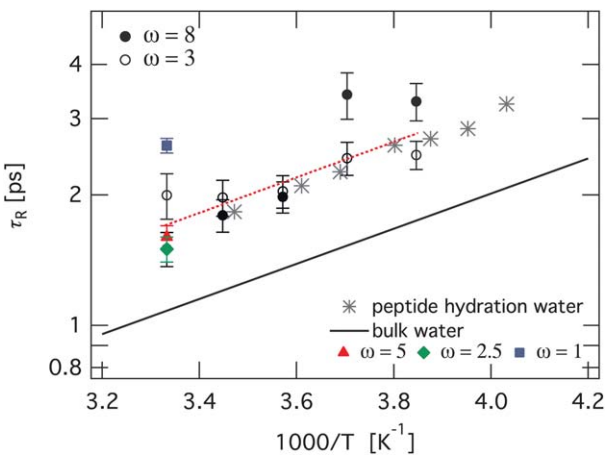

Fig. 2 Arrhenius plot of the rotational time τ_R for water in small and big reverse micelles. The shown temperature range corresponds to $312\ \text{K} \leq T \leq 240$ K. The black solid line shows bulk water,[23] grey stars correspond to rotational dynamics of water confined to peptides[26] and filled triangle, filled diamond and filled square represent results for water in reverse AOT micelles of different sizes.[11] The dotted line is the Arrhenius fit, eqn (9).

3.1 Rotational motion of water

The temperature dependence of the resulting rotational time $\tau_R = 1/(6D_R)$ is shown in Fig. 2 in the Arrhenius representation. By plotting the logarithm of τ_R *versus* $1000/T$ a thermally activated process with a single time constant gives a straight line as:

$$\tau_R = \tau_R^0 \exp(E_A/RT) \quad (9)$$

with the activation energy E_A, the gas constant R and the pre-factor τ_R^0. We compare our values for τ_R to QENS results obtained for bulk water (solid line),[23] water confined by peptides (stars)[26] and water in reverse AOT micelles of varying size comparable to our systems (filled symbols).[11] Even though our results scatter we note that they are in good absolute agreement with literature results for confined water. Results for water confined to reverse micelles of $\omega = 5$ and $\omega = 2.5$[11] and peptide hydration water[26] support our finding of a rotational water motion that is independent of the confining geometry. We interpret our results accordingly and we presume a water rotation independent of the droplet size. The simultaneous fit of τ_R for water in small and big droplets to eqn (9) is shown by the dotted line in Fig. 2. The fit yields an activation energy of $E_A = (1.9 \pm 0.4)$ kcal mol^{-1} and a pre-factor of $\tau_R^0 = (0.07 \pm 0.03)$ ps. In order to stabilize the subsequent fits we will from now on fix the rotational diffusion coefficient D_R to the averaged value determined by the Arrhenius fit. Let us emphasize that the determination of the translational width Γ_T is nearly unaffected by the exact value of D_R within the range where we fix it. When comparing the results for Γ_T obtained with imposed D_R to those with free D_R, we find that they agree within fitting error.

3.2 Translational motion of water as resolved by IN5

Let us now focus on the translational dynamics of the water molecules inside the droplets. All IN5 spectra are again fitted to eqn (8) but this time imposing D_R. In Fig. 3 we show the measured intermediate scattering function and fits for a selection of Q values for big and small droplets at $T = 271$ K. The translational widths Γ_T resulting from these fits are presented in Fig. 4 and show the typical jump diffusion behaviour as a function of Q^2. With higher temperature the widths Γ_T of both droplet sizes increase reflecting the increased translational mobility with increased temperature. For each temperature and Q the absolute value of Γ_T is smaller for water in smaller droplets than that of water confined to the bigger droplets.

Comparing Γ_T for water in small and big droplets to bulk water[23] measured at $T = 270$ K in Fig. 5 we note that the confined water in both droplets is on average slower than in the bulk. For the quantitative discussion of the dynamics of confined water we need to account for the diffusion of the reverse micelles in the oil matrix in order to distinguish between the confined water being moved along by the diffusing droplet and the translational motion of the water inside the droplet. These two translational processes are independent of each other and the total translational width is the sum of both Γ_{H_2O} and Γ_{drop}. The droplets perform free diffusion characterized by the diffusion coefficient D_{drop}. Assuming jump diffusion eqn (4) for the water inside the droplets we obtain for the total translational width:

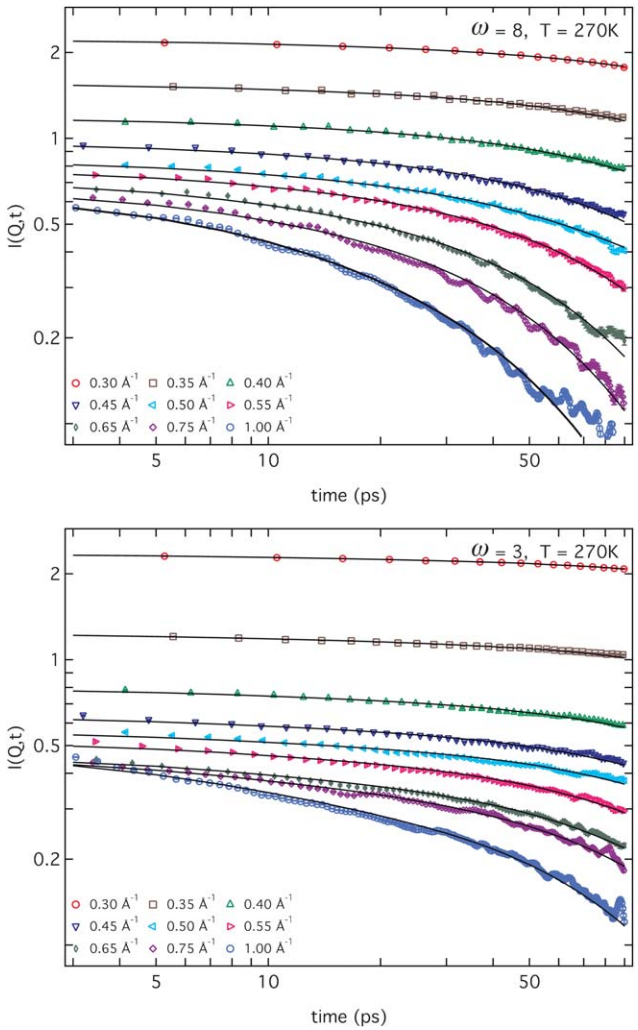

Fig. 3 Intermediate scattering function $I(Q, t)$ of water in big droplets (top figure) and small droplets (bottom figure) at $T = 270$ K measured on IN5. Lines are simultaneous fits to eqn (8) with a fixed rotational diffusion coefficient D_R.

$$\Gamma_T = \Gamma_{drop} + \Gamma_{H_2O}$$

$$= D_{drop}Q^2 + \frac{D_T Q^2}{1 + \tau_0 D_T Q^2} \quad (10)$$

The temperature dependent droplet diffusion coefficient D_{drop} in toluene is known from a recent neutron spin echo (NSE) study.[19] The measured diffusion coefficient D_{drop} of big droplets ($\omega = 8$) serves as well to calculate D_{drop} for the small droplets ($\omega = 3$) based on the Stokes–Einstein relation. Fig. 5 shows the corresponding T_{drop} for both droplet sizes at $T = 270$ K. Note that for the small droplets the measured width Γ_T is only slightly larger than the corresponding estimated Γ_{drop}. Even though this difference is larger in the case of the big droplets it is obvious that we need to consider the droplet diffusion in both cases. Neglecting the droplet diffusion would lead to a strong overestimation of the translational motion of the confined water molecules.

We fit the measured translational width Γ_T to eqn (10) with D_{drop} fixed to the values determined by NSE. Resulting fits are shown by solid lines in Fig. 5. The obtained translational diffusion coefficient D_T and the residence time τ_0 of confined water are shown in Fig. 6 as a function of temperature; the values are listed in Table 2. Again we compare our results for water in small (open circles) and big droplets (filled circles) to bulk water (stars)[23] and water confined to reverse AOT micelles with $\omega = 5$ (triangle).[11]

On average, confined water molecules diffuse slower than in bulk inside droplets of both sizes. The translational motion slows with decreasing droplet size, reflected by a decreasing translational diffusion constant D_T and an increasing residence time τ_0 with decreasing ω. Compared to bulk water the residence time τ_0 is prolonged about a factor of 10 and 100 for water inside big and small droplets respectively. It is worth noting that the observed temperature dependence of D_T for confined water is rather weak when compared to that of bulk water. We now compare our results to recently published values for water inside reverse AOT micelles with $\omega = 5$.[11] Note that the droplet size is in that case between those studied by us. The cited QENS experiments were carried out at $T = 300$ K and yielded $D_T = (0.5 \pm 0.1)$ cm^2 s^{-1} and $\tau_0 = (12 \pm 4)$ ps. Both values lie between our respective results at this temperature. This further confirms the systematic slowing of the translational motion with decreasing micelle size.

Let us recall that the QENS signal is due to all protons in the sample. QENS does not follow a single water molecule and therefore the shown results have to be understood as average values over all water molecules inside the reverse micelles.

3.3 Slower processes resolved by BASIS and IN16

We will now turn our attention to longer time scales probed by BASIS and IN16. Fig. 7 displays the intermediate scattering function $I(Q,t)$ obtained by combining data from all three spectrometers. The dotted lines show the above described fits obtained for short times on IN5, but now extrapolated to longer times. Whereas the rotational translational model (eqn (8)) also describes the long time data obtained for water in small droplets the model is insufficient in the case of water in bigger droplets. Here the model decays much faster than the data. The deviation between data and model at longer times implies that there must be an additional slower process in the case of water in big droplets that was not resolved by IN5.

Results from other experimental techniques showed that there exist different fractions of water inside reverse micelles.[27] For swollen reverse micelles of sufficient size a layer of slow water bound by the AOT was observed together with a faster water core. We therefore modify the model accordingly by adding a second term to eqn (8) to describe the observed slower decay at longer times:

$$I(Q,t) = I_{slow}(Q,t) + I_{fast}(Q,t)$$

$$= \frac{K}{1 + \frac{A}{B}}\left[A_0(Qa)e^{-\Gamma_T^B t} + A_1(Qa)e^{-(\Gamma_T^B + 2D_R)t}\right]$$

$$+ \frac{K}{1 + \frac{B}{A}}\left[A_0(Qa)e^{-\Gamma_T^A t} + A_1(Qa)e^{-(\Gamma_T^A + 2D_R)t}\right] \quad (11)$$

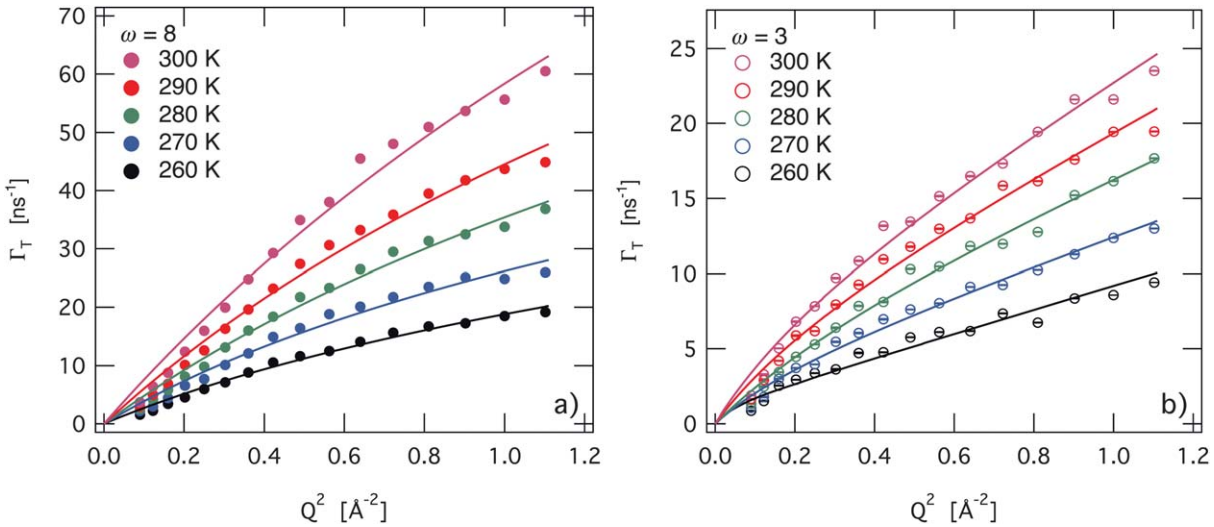

Fig. 4 Translational component Γ_T obtained from fitting of IN5 data with fixed D_R to eqn (8). Γ_T for water in a) big droplets and b) small droplets. Solid lines are fits to eqn (10) assuming free translational diffusion of the entire droplets and jump diffusion for the water molecules.

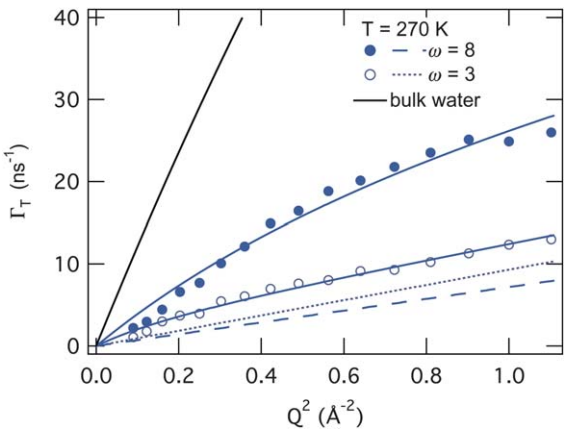

Fig. 5 Translational component Γ_T of small and big droplets at $T = 270$ K from fit of eqn (8) to IN5 data with fixed D_R. For comparison we show the translational component of bulk water at $T = 273$ K[23] and the calculated widths due to free droplet (dashed/dotted lines) diffusion measured by NSE and assuming $\Gamma_{drop} = D_{drop}Q^2$.[19] Solid lines are fits to eqn (10).

Indices A and B stand for fast and slow water respectively. Note that we consider rotational terms up to $l = 1$.

Eqn (11) is now used to fit the combined data sets with D_R again fixed to the value determined from the IN5 data. Within the errors we do not observe a systematic variation of $\frac{A}{B}$ neither with temperature nor with Q value. We recall that we only possess IN16 data for $T = 270$ K. We thus average $\frac{A}{B}$ assuming that the fraction of retarded water molecules does not change significantly with temperature. We obtain $\frac{A}{B} = 1.02 \pm 0.03$, which corresponds to $A \approx B \approx 4$ water molecules per AOT molecule, as the total number of water molecules per AOT molecule is equal to $\omega = 8$. Identifying the slow fraction of water molecules with the molecules that compose the water layer bound to the AOT this quantitatively means that each AOT molecule dynamically binds on average about 4 water molecules. This number is in the range of published values determined from other experimental methods including DSC, NMR and IR.[28–31] Furthermore the result of about 4 closely bound water molecules per AOT explains the observation that spectra of water in the small micelles ($\omega = 3$) can be described by the model (eqn (8)) which contains only one fraction of water. Apparently in those micelles all water is bound and therefore no fast core water is observed.

The combined spectra of water in the $\omega = 8$ system were then again fitted to eqn (11) but this time imposing $\frac{A}{B} = 1$ to stabilize the fitting procedure. In Fig. 7 a) combined data from all three spectrometers for water in big droplets at $T = 270$ K together with the resulting fits (solid lines) are shown. For a direct comparison the previous fits to eqn (8) are also included (dotted lines). The data at times $t > 100$ ps are now well described by the model and we obtain two translational widths Γ_T^A and Γ_T^B for the fast and slow water molecules respectively. These two widths are plotted as a function of Q^2 in Fig. 8 for temperatures $T = 270$ K, 280 K and 290 K, respective values are listed in Table 3. We also show the before obtained width Γ_T extracted from the analysis of the IN5 data alone (solid line). The width $\Gamma_{drop} = D_{drop}Q^2$ due to only droplet diffusion is displayed by the dotted lines. The two broken lines show the dependence of bulk water at a temperature 10 K below the temperature at which the confined water spectra were measured. The lower dashed lines show the measured width for bulk water after ref. 23, the upper line contains the broadening due to droplet diffusion. For all three temperatures we note that the translational diffusion of the fast water fraction is slowed compared to bulk water. The slowing down corresponds to a temperature shift of 10 K. This is in agreement with the observation that dynamics of water confined by peptides is similar to that of bulk water about 10–30 K lower.[23,32] For the slow water fraction we find that the translational diffusion Γ_T^B i) is slower than what would be deduced from fits at shorter times on IN5 only, ii) is still significantly faster than what we would expect

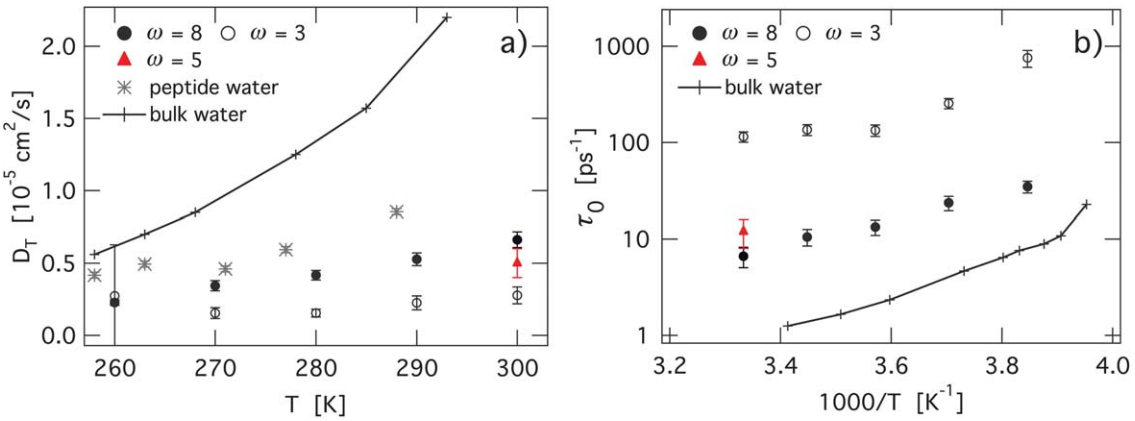

Fig. 6 a) Temperature dependence of the translational diffusion coefficient D_T for water in small and big reverse micelles. b) Arrhenius plot of the translational residence time τ_0 for temperatures from $T = 300$ K to 260 K. Lines between crosses correspond to results for bulk water[23] and grey stars show results for peptide hydration water.[26] With decreasing droplet size the translational motion becomes slower: D_T decreases and τ_0 increases the smaller ω gets.

from droplet diffusion alone (for $Q > 0.5$ Å^{-1}) and iii) follows a typical translational jump-diffusion Q dependence, implying that the water molecules inside the shell layer are not entirely immobilized on the timescale probed by QENS.

We want to emphasise the fact that only for $T = 270$ K and $Q = 0.3$ Å^{-1} and 0.5 Å^{-1} we possess data from all three spectrometers. For all other Q and T values the combined data consist of spectra from IN5 and BASIS only.

We interpret these results as follows: inside the big micelles there seem to be two fractions of water present. One fast fraction—called fraction A—behaves very similarly to bulk water. The respective translational width is within experimental accuracy undistinguishable from what was measured for bulk water at a temperature 10 K lower. As the number of points for both Γ_T^A and Γ_T^B, is restricted to only four we will not deduce diffusion constants D_T nor residence times τ_0 for this two-water-populations model.

3.3.1 Alternative models. Piletic and co-workers investigated water inside reverse AOT micelles by means of IR spectrosopy.[31] Micelle size dependent water spectra were reproduced by a weighted sum of bulk and bound water spectra. In this core–shell model the properties of the shell water were taken to be those of the water inside $\omega = 2$ micelles. We tested if our QENS data can be interpreted accordingly. For this purpose we tried to fit the intermediate scattering function $I(Q, t)$ of water in big micelles by a weighted sum of spectra for bulk and bound water. Bulk water parameters were taken from ref. 23; for the bound water fraction we used the spectra of water inside the small micelles corrected for droplet diffusion. As the only free parameter we varied the weighting of the bulk and bound fraction. This bulk-core + bound-shell model could not describe our QENS data in a satisfactory way.

As an alternative model to describe translational motion especially of supercooled and confined water we also need to mention the recently developed relaxing cage model (RCM) by Chen and co-workers.[33–35] The RCM model uses ideas from the mode-coupling theory and it is based on the assumption that in supercooled water each molecule is confined to a tetrahedrally coordinated hydrogen-bonded cage for a certain relaxation time. The translation of a water molecule therefore requires the rearranging of a large number of neighboring water molecules and the translational diffusion is thus strongly coupled to the local structural relaxation. In that case the intermediate scattering function can be written as a stretched exponential:

$$I_{RCM}(Q,t) = F_V(Q,t)\exp\left[-\left(\frac{t}{\tau}\right)^{\beta}\right] \quad (12)$$

where the pre-factor $F_v(Q, t)$ describes short time dynamics (<2 ps) as vibrations of the water molecules in the cage[6] and the stretched exponential describes the α-relaxation process of the cage build of the neighboring molecules. The lower the temperature is, the more β should deviate from one.[26]

Taking into account the rather large uncertainties in our data especially at higher Q and longer times we decided not to apply the RCM for the analysis of our data. The RCM model is

Table 2 Translational diffusion coefficient D_T and residence time τ_0 for water in small and big droplets. Values result from fits of IN5 data to eqn (8) with imposed rotational diffusion coefficient D_R. These results are displayed in Fig. 6.

		T/K				
ω		260	270	280	290	300
3	$D_T/10^{-5}$ cm^2 s^{-1}	0.27 ± 0.35	0.15 ± 0.04	0.15 ± 0.03	0.23 ± 0.05	0.28 ± 0.01
	τ_0/ps	757 ± 150	255 ± 31	134 ± 18	135 ± 17	115 ± 14
8	$D_T/10^{-5}$ cm^2 s^{-1}	0.23 ± 0.02	0.34 ± 0.03	0.42 ± 0.03	0.53 ± 0.04	0.66 ± 0.05
	τ_0/ps	35 ± 5	24 ± 4	13 ± 2	11 ± 2	7 ± 2

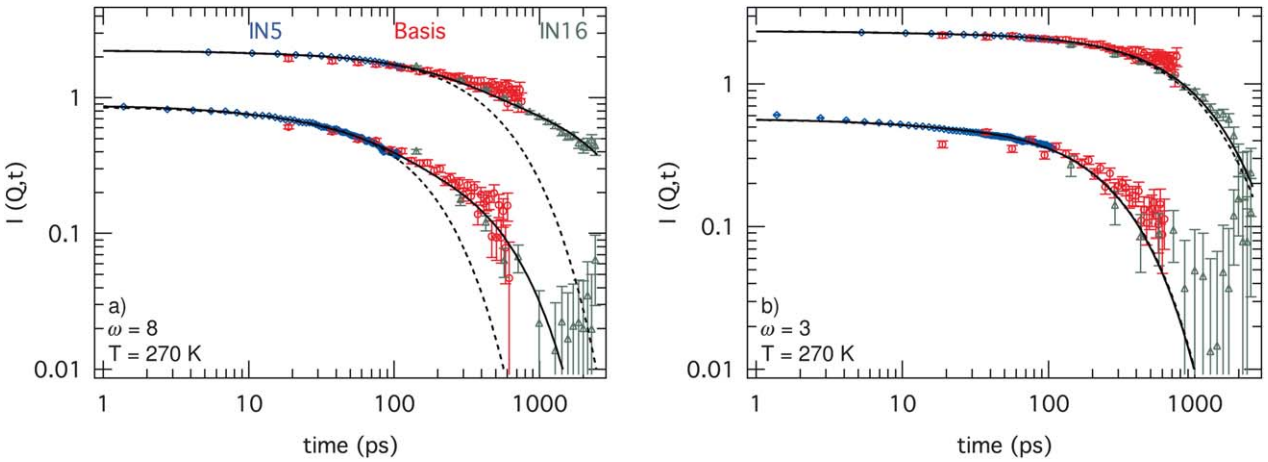

Fig. 7 Intermediate scattering function $I(Q, t)$ for water in big (a) and small (b) droplets combining data from IN5, BASIS and IN16 at $Q = 0.3$ Å^{-1} (upper curve) and $Q = 0.5$ Å^{-1} (lower curve). Solid lines are fits to the model with two water fractions assuming the same fraction of fast and slow water molecules. The dotted lines show the earlier fits to eqn (8) considering only one fraction of water molecules. a) Big droplets with $\omega = 8$, $\phi = 0.1$: Note that both models differ only at longer times $t > 100$ ps. b) Small droplets with $\omega = 3$, $\phi = 0.1$: The signal can be described over the entire tested time range by eqn (8). Dotted black lines show the fit considering only data from IN5, black solid lines show the fit to the same model taking into account all data. For $Q = 0.3$ Å^{-1} a slight difference can be observed, at $Q = 0.5$ Å^{-1} both fits are indistinguishable.

designed for water in the supercooled regime where we do not yet possess data at various temperatures. Moreover with this model it is not straightforward to take into account the dynamics of the entire diffusing droplets which are in our case essential.

Using the well-established rotational–translational model, eqn (8), we were able to compare our results to results obtained by other groups, who applied exactly the same model. Especially dynamic properties of bulk water as investigated by QENS were directly comparable.[23]

4 Discussion

The obtained results are of interest due to the resemblance of the reverse micelles with systems of biological relevance. We would now like to address the rather pure-science oriented question of whether the presented results show the signature of geometrical confinement effects. In our recently published study we used SANS and elastic scans on BS to investigate water freezing inside reverse AOT micelles of varying sizes.[18,19] We tested the structural stability of these droplets with decreasing temperature and we found that the water supercooling increases with decreasing micelle size. The absolute amount of supercooling could be described in a quantitative way by the Gibbs–Thomson equation which relates the droplet size to the maximum possible size of an ice nucleus. The structural behavior thus seems to be affected by the finite size. But how about the behavior of the relaxation times of water inside the micelles?

For pure geometrical confinement one expects to observe a decrease of the relaxation time, *i.e.* an accelerated motion of the confined molecules. The basic idea is that in the bulk liquid correlations between neighboring molecules influence the single molecule dynamics. While at high temperature the thermal energy is large enough to easily overcome local potentials arising from surrounding molecules, at lower temperature the influence of the neighbor interaction becomes more stronger. For most simple liquids the increasing importance of the neighbor potential with decreasing temperature leads to an exponential, *i.e.* Arrhenius increase of the viscosity and to single exponential relaxation functions until the system crystallizes (see eqn (9)). Static and dynamic heterogeneities, which are characteristic for glass forming liquids, lead for supercooled liquids to a viscosity which increases with decreasing temperature according to a Vogel–Fulcher law, *i.e.* stronger than for an Arrhenius dependence. It looks like the activation energy would continuously increase with decreasing temperature. There are many ideas describing this observation which is characteristic for a complex energy landscape. One major idea, first presented by Adams and Gibbs,[36] is that there are cooperative re-arranging regions (CRR) that influence the single molecule motion. The size of the CRR thus corresponds to the length scale above which molecules can be considered as moving independently of each other. The growing size of this region leads with decreasing temperature to the observed dramatic increase of the viscosity. The idea of geometrical confinement is now that enclosing the glass forming liquid in a restricted environment should prevent the size of this region from continuously growing, as the maximum size of a CRR is limited by the size of the confining space. Below a certain temperature the individual molecule may thus move faster than in bulk because fewer other molecules have to re-arrange.[36] But this scenario should be valid only if we could cut off the interaction to the environment, which is probably unphysical because walls always contribute to the interaction. Mostly a slowing-down of the dynamics in confinement is observed when hard wall effects dominate, *i.e.* for the case of interaction with slow walls.[1–3] An acceleration of the dynamics was observed either for hard confinement with hydrophobically treated walls (Alba-Simionesco *et al.* in ref. 2) or in soft confinement.[37] In our soft confined system the surrounding oil is also much faster than the water dynamics at the same temperature but water is separated by the AOT shell from the oil. Thus the shell dynamics itself is relevant for the wall interaction. From NSE we know that the time scale of shell deformation modes is

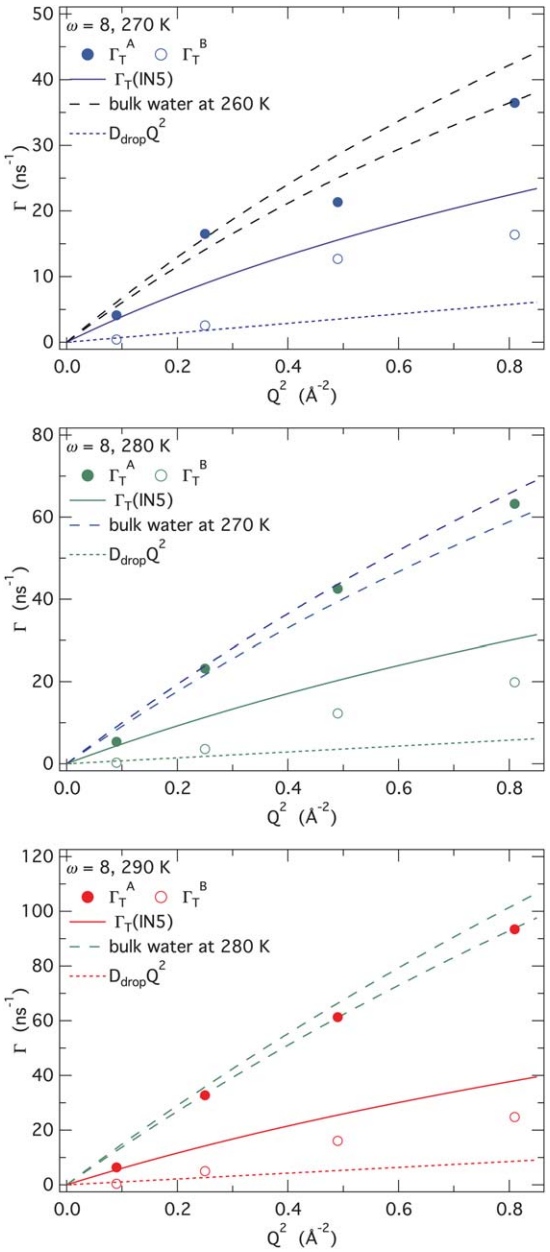

Fig. 8 Splitting of the translational component of water confined to big droplets at $T = 270$ K, 280 K and 290 K. Translational widths Γ_T^A and Γ_T^B of fast and slow water fractions as a function of Q^2. The solid lines show the single width Γ_T as before obtained from fits of IN5 data. Broken lines correspond to bulk water at a temperature 10 K lower[23] (with and without taking into account the droplet translation). Dotted lines show the width $D_{drop}Q^2$ due droplet diffusion. Fitting errors are smaller than symbols.

long compared to the time scale of water motion.[19] The slow AOT shell motion should therefore rather decrease the water mobility, which is what we observe. Moreover molecular dynamics simulation focusing on water in ionic micelles with varying counterions showed that the dynamical properties of water strongly depend on the type of the counterion.[38] This conclusion is in contrast to mid-IR spectroscopy experiments comparing water confined by ionic and non-ionic reverse micelles demonstrating that the only perturbation of the water dynamics is caused by the confinement itself and not by the counterion.[39] Another important question concerns the length-scale over which the wall dynamics influences the dynamics of the enclosed water molecules. Assuming we would have only a single hydration layer of water disturbed by the AOT shell, real geometrical confinement could then eventually be realized for the core water and we could expect this water to be accelerated compared to bulk water. But why do we observe a slowing-down of all water inside the micelles? (We recall that even in the bigger micelles the faster water fraction was slowed down compared to bulk water at the same temperature.) The most probable explanation is that the two-fraction model is too simple. Wall effects are expected to decrease quickly towards the interior of the droplet but they are very likely still noticeable in the middle of the droplet core. A smooth gradient from very slow relaxation times close to the AOT shell to faster relaxation times probably approaching those of bulk water in the center of large droplets could be more realistic and neutrons average of course over all the core content. Thus again, like in most confinement studies, wall effects seem to play an important role also in soft confinement and the ideal situation of a purely geometrical confinement is not achieved by reverse micelles. Nevertheless soft confinement has advantages, some of them were already mentioned: the confinement size is easily tunable, the interaction between different droplets can be varied and the viscosity of the surrounding oil can be changed (though this change is mediated by the surfactant shell to the confined liquid). Contrary to hard confinement, density and pressure changes between confined and bulk liquid can be neglected in soft confinement.

5 Summary and conclusions

Combining the three QENS spectrometers IN5, BASIS and IN16 we characterized the dynamical behavior of soft confined water over more than three decades in time from pico- to nanoseconds. By preparing microemulsion samples with $\omega = 8$ and $\omega = 3$ we studied the influence of confinement size on the water dynamics. The water signal was accessed by subtracting background spectra from fully deuterated samples with otherwise identical composition.

The rotational diffusion coefficient D_R of water was deduced from the short time data of IN5. We observed the rotation to be within the errors independent of droplet size. Assuming an Arrhenius behavior of the rotational time τ_R we found an activation energy of $E_A = (1.9 \pm 0.4)$ kcal mol^{-1} which is close to the bulk water value. Our results for τ_R agree with results for water confined by peptides[26] and reverse micelles.[11] Translational motion of water as resolved by IN5 follows a jump diffusion dependence. The average translational mobility of water inside reverse AOT micelles was reduced with comparison to bulk water at the same temperature and with decreasing droplet size an increasing slowing down of the translation was observed: the diffusion constants D_T decreased with decreasing droplet size whereas residence times τ_0 increased with decreasing droplet size. These results are in agreement with QENS results for water confined to reverse AOT micelles with $\omega = 5$.[11]

Taking into account BS data we extended the probed time range up to several thousands of picoseconds. Whereas data for

Table 3 Fitting results for water in $\omega = 8$ micelles. Combined analysis of data from TOF (IN5) and BS (BASIS and IN16) with eqn (11) imposing $\frac{A}{B} = 1$. Γ_T^A and Γ_T^B denote the translational widths of fast and slow water component. Fitting errors are smaller than 0.001 ps^{-1}. These results are displayed in Fig. 8 (only for $T = 270$ K and $Q = 0.3$ $Å^{-1}$ and 0.5 $Å^{-1}$ we possess IN16 data, results for other temperatures and scattering vectors are obtained from the analysis of IN5 + BASIS data).

	Γ_T^A/ps^{-1}				Γ_T^B/ps^{-1}			
T/K	$Q = 0.3$ $Å^{-1}$	$Q = 0.5$ $Å^{-1}$	$Q = 0.7$ $Å^{-1}$	$Q = 0.9$ $Å^{-1}$	$Q = 0.3$ $Å^{-1}$	$Q = 0.5$ $Å^{-1}$	$Q = 0.7$ $Å^{-1}$	$Q = 0.9$ $Å^{-1}$
270	0.004	0.017	0.021	0.036	<0.001	0.003	0.013	0.016
280	0.005	0.023	0.042	0.063	<0.001	0.004	0.013	0.020
290	0.006	0.033	0.061	0.093	<0.001	0.006	0.016	0.025

water inside small droplets was well described by the model extrapolated from shorter times accessed by IN5, in the case of big droplets we observed a significant difference. At longer times the intermediate scattering function decayed much slower than predicted by the fit to IN5 data where we considered only one fraction of water molecules performing rotation and translation. Taking into account the results from other experimental techniques which revealed two dynamically separated fractions of water corresponding to core and shell water we refined the fitting model. Spectra from water inside big micelles could successfully be described by a weighted sum of a fast (A) and a slow (B) component performing rotational translation motion. For the here studied micelles with $\omega = 8$ we found $A = B$ which corresponds to about 4 slow or bound water molecules per AOT molecule which is in absolute agreement with results from IR spectroscopy[40] and close to the number of 2 un-freezable water molecules per AOT as determined by SANS.[19] We found the translational behavior of the fast core component to resemble that of bulk water at a temperature reduced by 10 K. Also the slower water component shows translational motion that is still faster than what was estimated for the entire droplet diffusion. The scenario is sketched in Fig. 9. Contrary to IR spectra[31] our QENS spectra could not be reproduced by a weighted sum of bulk and bound water spectra.

QENS measures quantities averaged over all protons in the sample volume. Nevertheless, due to the large range of probed time scales we could distinguish between two fractions of water molecules which are very different with respect to their dynamical behavior. Whereas the existence of fast and slow water molecules was observed by MD simulations and other techniques[31,40] that probe mainly the vibrational behavior of water's hydrogen bonds, this is to our knowledge the first time that QENS experiments could evidence the existence of two water fractions inside reverse AOT micelles.

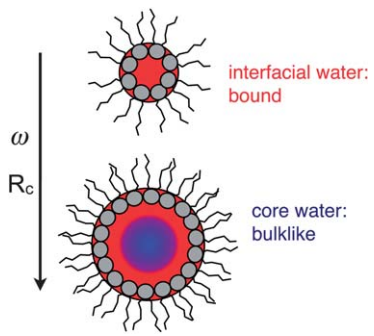

Fig. 9 Water inside small reverse micelles is bound to the AOT interface; with increasing radius the water in the micelle core behaves similarly to bulk water at a 10 K colder temperature.

Acknowledgements

We acknowledge the ILL for the allocated beam time and the co-financing of the PhD thesis of T.L.S. Financial support by the DFG (project number STU 191/4-1) is acknowledged. A portion of this research at ORNL's SNS was sponsored by the Scientific User Facilities Division, Office of Basic Energy Sciences, U.S. Department of Energy.

References

1 Proceedings of the International Workshop on Dynamics in Confinement, 2000.
2 Proceedings of the second International Workshop on Dynamics in Confinement, 2003.
3 Proceedings of the 3rd International Workshop on Dynamics in Confinement, 2007.
4 R. Zorn, L. van Eijck, M. M. Koza and B. Frick, *Eur. Phys. J. Spec. Top.*, 2010, **189**, 1–2.
5 E. Fratini, S.-H. Chen, P. Baglioni and M. Bellissent-Funel, *J. Phys. Chem. B*, 2002, **106**, 158–166.
6 L. Liu, C. Mou, C. Yen and S.-H. Chen, *J. Phys.: Condens. Matter*, 2004, **16**, S5403–S5436.
7 N. Malikova, A. Cadéne, V. Marry, E. Dubois, P. Turq, J.-M. Zanotti and S. Longeville, *Chem. Phys.*, 2005, **317**, 226–235.
8 E. Mamontov, C. Burnham, S.-H. Chen, A. Moravsky, C. Loong, N. de Souza and A. Kolesnikov, *J. Chem. Phys.*, 2006, **124**, 194703.
9 M. Rovere, editor, *J. Phys.: Condensed Matter*, 2004, **16**.
10 L. Wang, F. He and R. Richert, *Phys. Rev. Lett.*, 2004, **92**, 095701.
11 M. R. Harpham, B. M. Ladanyi, N. E. Levinger and K. W. Herwig, *J. Chem. Phys.*, 2004, **121**, 7855–7868.
12 R. Zorn, M. Mayorova, D. Richter and B. Frick, *Soft Matter*, 2008, **4**, 522–533.
13 M. van Dijk, J. Joosten, Y. Levine and D. Bedeaux, *J. Phys. Chem.*, 1989, **93**, 2506–2512.
14 W. Meier, *J. Phys. Chem. B*, 1997, **101**, 919–921.
15 M. Kotlarchyk, S. H. Chen and J. Huang, *J. Phys. Chem.*, 1982, **86**, 3273–3276.
16 M. Kotlarchyk, S. H. Chen, J. Huang and M. Kim, *Phys. Rev. A: At., Mol., Opt. Phys.*, 1984, **29**, 2054–2069.
17 S.-H. Chen, J. Rouch, F. Sciortino and P. Tartaglia, *J. Phys.: Condens. Matter*, 1994, **6**, 10855–10883.
18 T. Spehr, B. Frick, I. Grillo and B. Stühn, *J. Phys.: Condens. Matter*, 2008, **20**, 104204.
19 T. Spehr, B. Frick, I. Grillo, P. Falus, M. Müller and B. Stühn, *Phys. Rev. E: Stat., Nonlinear, Soft Matter Phys.*, 2009, **79**, 031404.
20 M. Bee, *Quasielastic Neutron Scattering: Principles and Applications in Solid State Chemistry, Biology and Materials Science*, Adam Hilger, 1988.

21 M Belletete, M. Lachapelle and G. Durocher, *J. Phys. Chem.*, 1990, **94**, 7642–7648.
22 S. H. Chen, P. Gallo, F. Sciortino and P. Tartaglia, *Phys. Rev. E: Stat. Phys., Plasmas, Fluids, Relat. Interdiscip. Top.*, 1997, **56**, 4231–4241.
23 J. Teixeira, M. Bellissent-Funel, S. Chen and A. Dianoux, *Phys. Rev. A: At., Mol., Opt. Phys.*, 1985, **31**, 1913–1917.
24 K. S. Singwi and A. Sjölander, *Phys. Rev.*, 1960, **119**, 863–871.
25 V. Sears, *Can. J. Phys.*, 1967, **45**, 237–254.
26 C. Malardier-Jugroot and T. Head-Gordon, *Phys. Chem. Chem. Phys.*, 2007, **9**, 1962–1971.
27 A. Dokter, S. Woutersen and H. Bakker, *Proc. Natl. Acad. Sci. U. S. A.*, 2006, **103**, 15355–15358.
28 C. Boned, J. Peyrelasse and M. Moha-Ouchane, *J. Phys. Chem.*, 1986, **90**, 634–637.
29 P.-O. Quist and B. Halle, *J. Chem. Soc., Faraday Trans. 1*, 1988, **84**, 1033–1046.
30 M. Freda, G. Onori, A. Paciaroni and A. Santucci, *Chem. Phys. Lett.*, 2001, **348**, 311–316.
31 I. Piletic, D. Moilanen, D. Spry, N. Levinger and M. Fayer, *J. Phys. Chem. A*, 2006, **110**, 4985–4999.
32 M. Bellissent-Funel, J.-M. Zanotti and S.-H. Chen, *Faraday Discuss.*, 1996, **103**, 281–294.
33 S.-H. Chen, C. Liao, F. Sciortino, P. Gallo and P. Tartaglia, *Phys. Rev. E: Stat. Phys., Plasmas, Fluids, Relat. Interdiscip. Top.*, 1999, **59**, 6708–6714.
34 J.-M. Zanotti, M.-C. Bellissent-Funel and S.-H. Chen, *Phys. Rev. E: Stat. Phys., Plasmas, Fluids, Relat. Interdiscip. Top.*, 1999, **59**, 3084–3093.
35 M.-C. Bellissent-Funel, *Eur. Phys. J. E*, 2003, **12**, 83–92.
36 G. Adam and J. Gibbs, *J. Chem. Phys.*, 1965, **43**, 139–146.
37 T. Blochowicz, E. Gouirand, A. Fricke, T. Spehr, B. Stühn and B. Frick, *Chem. Phys. Lett.*, 2009, **475**, 171–174.
38 S. Senapati and M. Berkowitz, *J. Phys. Chem. A*, 2004, **108**, 9768–9776.
39 J.-B. Brubach, A. Mermet, A. Filabozzi, A. Gerschel, D. Lairez, M. Krafft and P. Roy, *J. Phys. Chem. B*, 2001, **105**, 430–435.
40 A. Dokter, S. Woutersen and H. Bakker, *Phys. Rev. Lett.*, 2005, **94**, 178301.